Available online at www.sciencedirect.com
ScienceDirect
Cement & Concrete Composites 29 (2007) 279–289
Cement & Concrete Composites
www.elsevier.com/locate/cemconcomp

Bond and failure mechanisms of textile reinforced concrete (TRC) under uniaxial tensile loading

U. Häußler-Combe, J. Hartig *

Institute of Concrete Structures, Faculty of Civil Engineering, Technische Universität Dresden, D-01062 Dresden, Germany

Received 6 June 2006; received in revised form 20 December 2006; accepted 22 December 2006
Available online 19 January 2007

Abstract

Composites of technical textiles used as reinforcement and fine-grained concrete used as matrix, called textile reinforced concrete (TRC), provide the opportunity to construct thin structural elements. Typically, the reinforcing textiles are made of yarns consisting of hundreds of alkali-resistant glass filaments, which leads to a complex microstructural behavior, especially with respect to bond. In order to reveal its complexity some experimental investigations are summarized. It is recognizable that the bond between concrete and filaments is subject to some deficiencies. Therefore, mechanical models are required to describe the early failure of single filaments as well as the bond and friction behavior of filaments and concrete. The mechanical models are solved numerically within a finite element framework. Exemplary calculations for an ideal yarn and important cases of deficiencies show typical properties of the load carrying and the bond behavior.

Keywords: Textile reinforced concrete; Non-linear analysis; Bond; Slip; Cracking

1. Introduction

Alkali-resistant glass fibers (AR-fibers) have been used for a long time to improve concrete properties, especially failure properties and ductility. However, conventional short fibers with a diameter of about 15 μm and a length ranging from 5 up to 25 mm exhibit a random orientation within a cement matrix, which means that only a small fraction is efficiently used. Efficiency and utilization may be improved with continuous fibers or filaments respectively, which are tied into yarns. Furthermore, multi-filament yarns may be connected to two-dimensional structures with special binding techniques where the yarns may be given a desired direction according to the loading conditions, see Fig. 1. These flexible structures are called technical fabrics. The use of such fabrics as reinforcement in concrete leads to thin structural elements with high strength, high durability and corrosion resistance [2–5].

Compared to conventional reinforcement, special problems have to be regarded. A typical single filament has a diameter of about 13–15 μm, with up to 2000 filaments bundled into a circular or oval yarn. Upon embedding into a cement matrix, a separation of outer filaments from the bundle occurs, see Fig. 2. These separated filaments are fully embedded into the cement matrix and work as independent reinforcements. In contrast, central filaments of a yarn have no immediate connection to the matrix but contact neighbor filaments or remain partially unconnected, as cement slurry with its high viscosity cannot reach narrow spaces. All kinds of transitions can be seen in between these areas, with filaments partially connected to the matrix, partially contacting neighbors and partially remaining free. Each of these may occur with varying degrees [6].

In this context, bond behavior is different compared to that between reinforcing steel and concrete. Two types of bond have to be considered: bond between filaments and

* Corresponding author. Fax: +49 351 463 37279.
E-mail address: jens.hartig@mailbox.tu-dresden.de (J. Hartig).

0958-9465/$ - see front matter © 2007 Elsevier Ltd. All rights reserved.
doi:10.1016/j.cemconcomp.2006.12.012

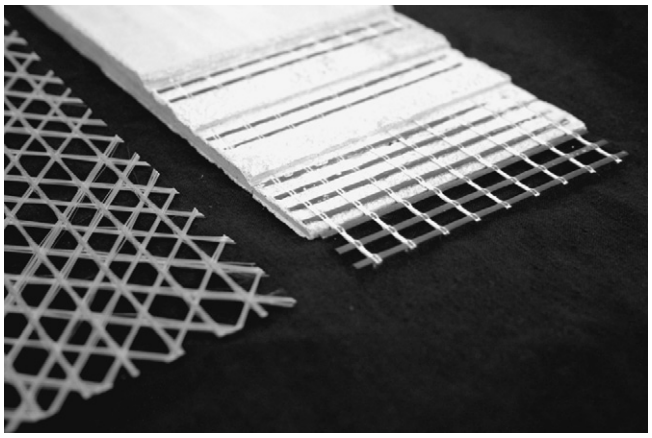

Fig. 1. Multi-axial fabric reinforcement and textile reinforced concrete; from [1].

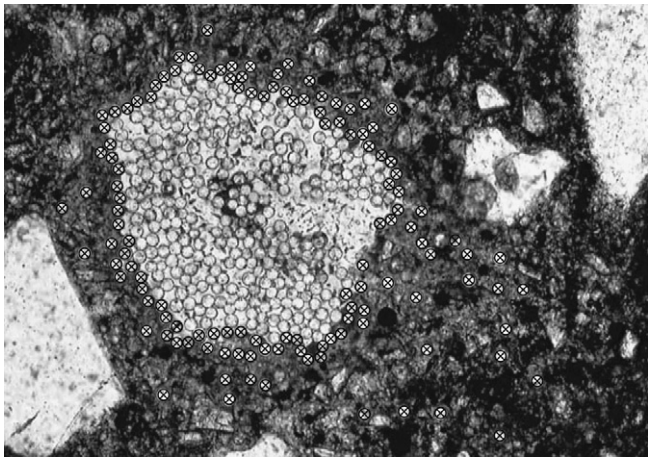

Fig. 2. Cross-section of a multi-filament yarn; separated filaments crossed out.

concrete; and bond between the filaments themselves. Regarding a particular filament, these types generally work simultaneously, and regarding different filaments of a yarn, the contribution of the bond types is different. Consequently, a multi-filament yarn embedded in a cement matrix constitutes a complex structure in itself, which leads to special properties of structural behavior if multi-filament yarns are used as reinforcement. This is demonstrated in Section 2 with experimental results of tension plates.

The complex structural behavior, especially with respect to bond, can be simplified with appropriate mechanical models. They should take into account effects such as the limited tensile strength of the materials and different types of non-linear bond. A mechanical model incorporating a simple geometry but complex physical properties is developed in Sections 3.1 and 3.2. The mechanical model is solved in a finite element framework, which is described in Section 3.4. In Section 4, the model is applied to a tension plate with unidirectional reinforcement of multi-filament yarns in several variations. First, a so-called ideal yarn, homogeneous over its cross-section and continuously connected to the concrete component along the longitudinal direction, is described in Section 4.1. This ideal yarn is used as a reference for bond mechanisms such as slip of filaments, discontinuous connections or premature failure of filaments. All these cases are discussed in Section 4.2. It should be noted that it is not intended to achieve a perfect agreement between experimental and numerical results but to show how the aforementioned micromechanical mechanisms influence the macroscopic structural behavior. Finally, some conclusions are drawn in Section 5.

2. Experimental observations

Some essential properties of textile reinforced structures can be observed with tension bars or tension plates. Such experimental investigations were performed by Jesse and Curbach [7,8] and Hegger and Molter [9], which both show similar results. The experiments by Jesse [8] will be described and the following computations are referred to these experiments. A typical specimen is shown in Fig. 3. The concrete component has a fine-grained structure with a maximum aggregate size of 1 mm. Thus, the matrix has rather properties of a cement mortar than of a normal concrete. Nevertheless, the matrix of the composite is referred to as concrete in the following. The whole composition is given in Table 1. The glass material has to be alkali-resistant in order to sustain long-term embedding in a cement matrix [6]. The tension plates under consideration are reinforced with ARG310, a yarn type, which is commercially available and produced by Nippon Electric Glass (NEG). Each yarn has 800 filaments and its size is measured with 310 tex, which indicates its unit length weight (1 tex = 1 g/km). With a specific weight of $\varrho = 2.817\ \mathrm{g/cm^3}$ this

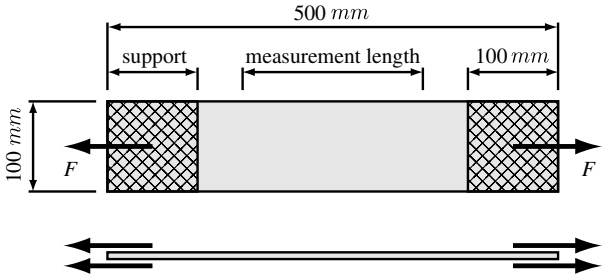

Fig. 3. Tension plate specimen; schematic.

Table 1
Composition of fine-grained concrete

Component	Mass ratio of aggregates (–)	Quantity (kg/m^3)
Aggregates (sand, max. size 1 mm)	1.000	942.0
Cement	0.667	628.0
Fly ash	0.282	263.8
Microsilicate (in suspension)	0.055	50.2
Water (total content)	0.333	313.7
Plasticizing agent	0.013	12.2

Table 2
Material parameters

	Concrete	Filament
E (MN/m^2)	30,000	80,000
f_t (MN/m^2)	7	2270
ϵ_t (–)	0.23×10^{-3}	28×10^{-3}

corresponds to a cross-sectional area of $A_y = 0.110$ mm^2 for each yarn. The yarns are arranged in 3 up to 6 layers in a plate of 8 mm thickness. Within a layer, lateral distances between yarns of 3 and 6 mm typically exist. This results in reinforcement ratios from 1% to 3%. The mean strength properties of the concrete and the filaments are given in Table 2.

The specimen is fixed in a hydraulic testing machine by pivoted wedge clamps, see Fig. 3. The displacements are measured along a base length of 200 mm on both sides of the specimen in the longitudinal direction with a clip on measuring device. Loading is applied by displacement control with a rate of 0.015 mm/s. A typical result is shown in Fig. 4 where the measured load has been related to the plate's cross-sectional area, which leads to the mean stress $\bar{\sigma}$, and the measured displacement has been related to the measurement base length, which leads to the mean strain $\bar{\epsilon}$. In principle, the stress–strain behavior of textile-reinforced concrete is similar to concrete with steel rebars. Three typical states can be observed: state I where the concrete remains uncracked until the tensile strength is reached, state IIa with formation of concrete cracks with a flat slope of the stress–strain relation and state IIb, which is the final cracking state with highly reduced stiffness compared to state I. In contrast to rebars, a state of yielding does not occur as the ultimate failure of a cross-section with all yarns occurs without distinct preannouncements. Furthermore, the following characteristic effects can be observed:

– Suppression of cracks: Nominal initial cracking stresses of the tension plate are higher compared to values, which can be determined with uniaxial elasticity assuming that the concrete cracks if the stress of the composite exceeds the tensile strength of the concrete. This is explained with non-homogeneous strain distributions combined with particular fracture mechanisms. With the described test configuration, [8] found an increase of the initial cracking stresses of about 30% with a reinforcement ratio of about 3%.
– Deficit of stiffness: Regarding state IIb, the actual stiffness of the cracked tension plate is lower compared to the nominal stiffness of the whole bulk of filaments alone. This is probably caused by the premature failure of a certain portion of filaments and by premature debonding of core filaments [8,10].
– Deficit of tension stiffening: Tension stiffening is measured in reinforced concrete as horizontal shift of the stress–strain line in state IIb to a parallel line through the origin. It is caused by the participation of the concrete between concrete cracks. The experimental values observed by [8] are lower compared to theoretical values according to the theory of ordinary reinforced concrete [11]. This might be caused by an initial waviness of filaments, which have to be lined up straightly before carrying loads [8].
– Complex failure behavior: The filament strength is higher compared to the yarn strength while the yarn strength is generally higher than the nominal tension plate strength. This is explained with the highly non-homogeneous and partially discontinuous stress distribution in a yarn combined with the low ductility of single filaments.

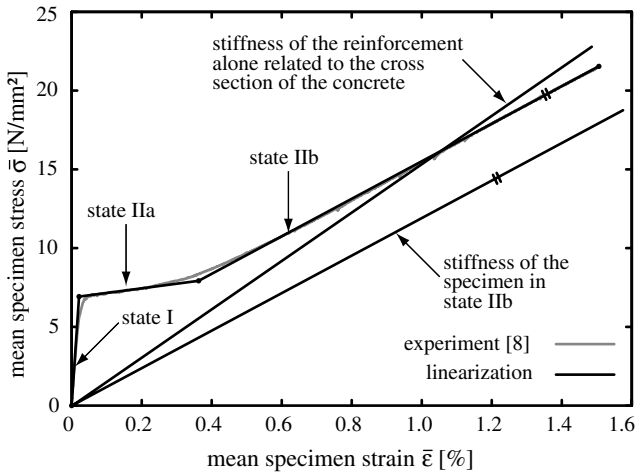

Fig. 4. Typical experimental stress–strain relation of a tensile plate.

In a first approach, these effects may be classified either as uniaxial or multi-axial. A description of multi-axial properties, as in case of crack suppressions, necessarily requires 2D or 3D models. However, uniaxial properties may be reduced to degrees of freedom in the longitudinal direction where non-homogeneous cross-sectional properties may be regarded by splitting them into several coupled uniaxial components. This is presumably the case with stiffness deficit, tension stiffening deficit and complex failure behavior. Only the uniaxial approach is used here, with the following mechanisms included for a proper description of textile reinforced concrete:

– Delayed loading of filaments with initial stressless displacements.
– Indirect loading of core filaments with load transmission by sleeve filaments.
– Different bond behavior for the interaction between concrete and filaments on the one hand and between filaments themselves on the other hand.
– Premature failure of single filaments and redistribution of forces within the yarn.

Uniaxial mechanical models incorporating these mechanisms will be described in the following.

3. The mechanical model

3.1. Basics

The basic property of textile reinforcement is given by the fact that a yarn cannot be considered as homogeneous over its cross-section. Thus, it is divided into so-called segments. In principle, the number of segments may vary from one, i.e. a case comparable to a steel reinforcement bar, to the number of filaments forming a yarn, i.e. each filament is modeled separately. If appropriate, a group of filaments may be treated together as one segment, which is homogeneous over its cross-section by definition. In Fig. 5, a possible segmentation in sleeve (tangential) and core (radial) direction is shown. For the modeling, the segments are arranged schematically like a matrix, which is also shown in Fig. 5. The concrete component is also considered as homogeneous over its cross-section. The elements of the yarn segments and the concrete component are connected with bond elements at the nodes, see Fig. 5. The whole system has a simple geometry but should contain physical non-linearities such as non-linear bond as well as limited concrete and reinforcement tensile strengths. Furthermore, the segmentation of the reinforcement leads to complex mechanical and geometrical relations.

Given a total cross-sectional area A of a yarn, this area has to be divided into the cross-sectional areas A^{ij}, where i indicates the ith segment row and j indicates the jth segment column. The following approach is chosen:

$$A^{ij} = \alpha^{ij} \cdot A, \tag{1}$$

where the weight coefficients α^{ij} describe the fraction of the area of a segment ij and have to fulfill the condition $\sum \alpha^{ij} = 1$. Bond between the segments is ruled by a relation

$$\tau = h(s) \tag{2}$$

with a bond stress τ and a slip s. The bond law h should be independent from geometric conditions and should only describe the behavior of different materials in interaction along surfaces. Surveys for possible bond laws for filaments and yarns are given by [12,13]. Bond stresses τ have to be multiplied by a circumferential value C to get length-related bond forces T between two components interacting with each other. This is applied to a segment ij with a circumference C^{ij}. The interaction with its upper neighbor $(i-1,j)$ leads to a bond force per unit length:

$$T_t^{ij} = C^{ij}[\beta_{\mathrm{CF},t}^{ij} h_{\mathrm{CF}}(s_t^{ij}) + \beta_{\mathrm{FF},t}^{ij} h_{\mathrm{FF}}(s_t^{ij})]. \tag{3}$$

Two types of bond laws are introduced, $h_{\mathrm{CF}}(s)$ for concrete–filament interaction and $h_{\mathrm{FF}}(s)$ for filament–filament interaction where s is the slip between a segment and its neighbors. The coefficients $\beta_{\mathrm{CF},t}^{ij}$ and $\beta_{\mathrm{FF},t}^{ij}$ respectively rule the weight of each interaction type in the top interface of the segment ij. The same approach is chosen with respect to Fig. 5 for the left $(i,j-1)$, right $(i,j+1)$ and bottom $(i+1,j)$ interfaces of the segment ij with a complete set of neighbors where the index t in Eq. (3) is replaced by l, r or b respectively. Furthermore, the conditions $T_l^{ij} = T_r^{i,j-1}$, $T_t^{ij} = T_b^{i-1,j}$, $T_r^{ij} = T_l^{i,j+1}$ and $T_b^{ij} = T_t^{i+1,j}$ hold.

The choice for a circumferential value C requires some attention. A circular cross-sectional area A leads to the circumference $C_{\mathrm{circ}} = 2\sqrt{\pi A}$. However, groups of filaments or yarns do not have a circular shape but can show ellipticity and surface roughness. A first approach to a more realistic circumference is given by $\psi\omega C_{\mathrm{circ}}$ with a roughness coefficient ω and a shape coefficient ψ where $\psi = 1$ for circular shapes. This is assumed for the following if not otherwise stated. The roughness coefficient is estimated with $\omega \approx 3$ according to [8] where the circumferential lines of yarns embedded in concrete are determined by means of geometrical analysis of microscopic photographs. Altogether, this leads to the circumference for a segment

$$C^{ij} = 2\psi\omega\sqrt{\pi A^{ij}}. \tag{4}$$

Regarding Eq. (3) the weight coefficients besides $0 \leqslant \beta_{\mathrm{CF}}^{ij} \leqslant 1$ and $0 \leqslant \beta_{\mathrm{FF}}^{ij} \leqslant 1$ should satisfy

$$(\beta_{\mathrm{CF},l}^{ij} + \beta_{\mathrm{FF},l}^{ij}) + (\beta_{\mathrm{CF},t}^{ij} + \beta_{\mathrm{FF},t}^{ij}) + (\beta_{\mathrm{CF},r}^{ij} + \beta_{\mathrm{FF},r}^{ij}) + (\beta_{\mathrm{CF},b}^{ij} + \beta_{\mathrm{FF},b}^{ij}) + \beta_{\mathrm{void}}^{ij} = 1 \tag{5}$$

whereby a whole neighborhood of a segment ij is included with $\beta_{\mathrm{void}}^{ij}$ as the portion of void space. Therefore, only $\beta_{\mathrm{CF},l}^{ij}$ and $\beta_{\mathrm{CF},t}^{ij}$ have to be determined as a function of the position ij, as the relations $\beta_{\mathrm{CF},r}^{ij} = \beta_{\mathrm{CF},l}^{i,j+1}$ and $\beta_{\mathrm{CF},b}^{ij} = \beta_{\mathrm{CF},t}^{i+1,j}$ hold. Furthermore, it is feasible to assume $\beta_{\mathrm{CF},l}^{ij} = \beta_{\mathrm{CF},t}^{ij}$ because at one segment the same bond conditions should exist for concrete–filament bond for all interfaces. Thus, a value β_{CF}^{ij} remains to be determined as a function of its position within the yarn. The same arguments apply to filament–filament bond with β_{FF}^{ij}. Some formal modifications of this approach are necessary if a segment ij does not have a complete set of neighbors in the matrix scheme.

The values β_{FF}, β_{CF}, ψ, β have to be determined based on experimental investigations. However, in any case some extent of uncertainty has to be taken into account. So far, a model for a single yarn has been developed. In case of multiple unidirectional yarns, the geometric parameters A and

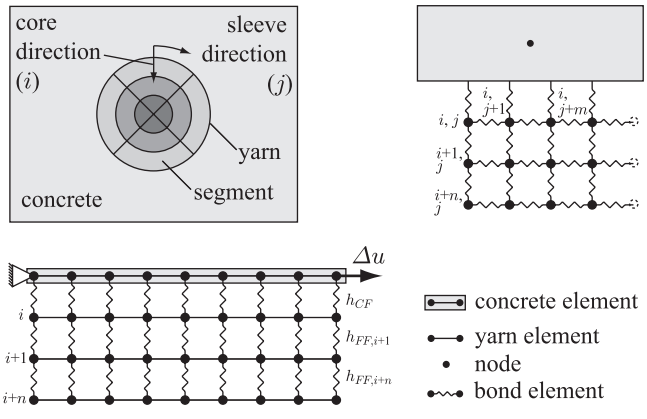

Fig. 5. Schematic description of mechanical model.

C have to be multiplied with the number of yarns n_y in the total cross-section of the tension plate.

3.2. Materials and geometries

Similar to steel rebars, bond laws between concrete and textile reinforcement are experimentally determined with pullout tests of multi-filament yarns or single filaments from concrete specimens. A typical bond law for the case of concrete–filament interaction formulated as the bond stress–slip relation $h_{CF,Ref}$ is shown in Fig. 6 with an increasing branch, a peak value τ_{max}, a decreasing branch, and finally a residual value τ_{res}. In principle, this is the same for filament–concrete bond and filament–filament bond but with different values for the maximum τ_{max} with the corresponding slip s_{max}, and the residual τ_{res} with the corresponding slip s_{res}. Some values are given in Table 3, which were chosen corresponding to experimental investigations [13,14]. As filament–filament interaction is mainly governed by friction, the bond law h_{FF} does not have a decreasing branch. Thus, the maximum and the residual bond stresses are assumed equal. As experimental data, especially regarding filament–filament bond, are rare, the described bond laws have to be regarded as first approaches and are open for further enhancement.

While the bond laws are highly non-linear, the material behavior of the yarn segments and the concrete component is assumed to be linear under tension with a limited tensile strength, see Table 2. For both materials, a perfectly brittle failure is assumed. Thus, the fracture energy of the concrete has been neglected in a first approach. Regarding filaments embedded in a cement matrix it is well known that portions of filaments suffer strength deteriorations due to particular chemical and mechanical influences. With the available experimental data, the values for this portion and the values for the reduced filament strength have to be considered as uncertain. Thus, the corresponding model parameters are used as variables in the later computations.

Besides the material data, some geometric properties have to be defined for the tension plate model. These properties are based on the dimensions of the specimen, see Fig. 3. The total length is 500 mm, which has been adopted for the concrete component and all yarn segments in the model. The concrete's cross-sectional area amounts to 800 mm^2. The yarns have been described in Section 2. The cross-sectional area of a single yarn is given with $A_y = 0.110$ mm^2, which leads to a circumference $C = 3.527$ mm with $\omega = 3$ and $\psi = 1$, according to Eq. (4). The number of yarns in a plate is chosen with $n_y = 140$ for the computations, which results in a reinforcement ratio of 1.9% and corresponds to a medium value compared to the experimental tension plates, see Section 2. Finally, a free length in the longitudinal direction, i.e. where tensile failure of concrete or filaments may occur in the model, is chosen with 300 mm. Apart from this free length, the plate is supported and fixed by lateral pressure from wedge clamps and is assumed as unbreakable.

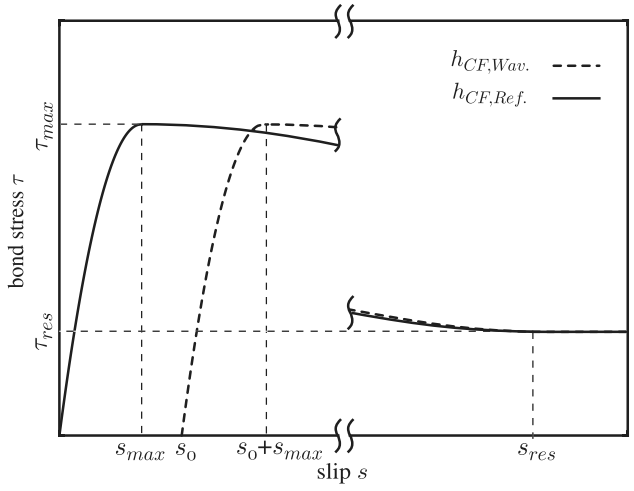

Fig. 6. Typical bond behaviors for concrete–filament interaction; schematic.

Table 3
Bond parameters

	Concrete–filament h_{CF}	Filament–filament h_{FF}
τ_{max} (MN/m^2)	3	1
s_{max} (m)	1×10^{-5}	1×10^{-5}
τ_{res} (MN/m^2)	1	1
s_{res} (m)	1×10^{-3}	–

3.3. Crack spacing

As concrete has a limited tensile strength, crack patterns will develop during loading, with crack widths and crack spacing being important characteristics. In the following, an estimation for crack spacing is given. In case of one single yarn segment, which is directly connected to the concrete component, stress transfer may be described by

$$A_C \mathrm{d}\sigma_C = n_y C \tau(x)\,\mathrm{d}x \tag{6}$$

with the longitudinal coordinate x, the number of yarns n_y, the circumference C of one yarn, the concrete's cross-sectional area A_C and the stress σ_C of the concrete. This equation may be extended to yarns with multiple segments, which is omitted here. Eq. (6) may be integrated starting at the position of a crack ($x = 0$) up to a distance $x = l_{ct}$ where the concrete tensile strength is reached. The mean bond stress is assumed with $\tau_{mean} = \gamma \tau_{max}$ with a bond utilization parameter $\gamma < 1$. With the concrete tensile strength f_{ct} this leads to

$$l_{ct} = \frac{A_C}{n_y C} \cdot \frac{f_{ct}}{\tau_{mean}}. \tag{7}$$

Given two adjacent cracks, a distance of at least $2l_{ct}$ is required for a new crack to occur in between. If a new crack occurs, it has a distance to existing cracks, which is greater

than or equal to l_{ct}. Thus, crack spacing a for final crack patterns may be estimated with

$$l_{ct} \leqslant a \leqslant 2l_{ct}. \tag{8}$$

With the values given in Section 3.2 and a concrete–filament bond law, one gets

$$l_{ct} = \frac{3.78}{\gamma}\ \text{mm}. \tag{9}$$

The bond utilization parameter γ can be estimated within some bounds. For example $\gamma = 0$ means no bond while $\gamma = 1$ means full bond. The parameter γ can also be taken from numerical calculations by relating the mean bond stress to its maximum value, see Fig. 12. A rectangular course as observable in Fig. 12 will lead to $\gamma \approx 1$ while a triangular course would lead to $\gamma = 0.5$. Thus, Eqs. (8) and (9) may be used to illustrate the bond and the cracking behavior of the different cases.

3.4. Numerical implementation and solution methods

A finite element framework is chosen for the numerical solution of the equations resulting from the mechanical model. The concrete component and each yarn segment are discretized with uniaxial bar elements with a common element length ΔL. In a cross-section, a nodal position is shared by a number of n_s nodes of the n_s yarn segments and the node of the concrete component, which are coupled by bond elements as shown in Fig. 5. According to Eq. (3), the force of the bond element between a segment ij and its top neighbor is given by

$$\overline{T}_t^{ij} = \Delta L \cdot T_t^{ij}. \tag{10}$$

For the bond elements that are positioned at the left, right or bottom interface the bond forces are given respectively by changing the index t into l, r or b.

Non-linear bond laws and limited tensile strengths lead to a non-linear problem. This is computed with an incremental loading, with equilibrium iterations being performed in each loading step. Loading is applied with increasing prescribed displacements of the outmost right concrete node at $x = L$ while the outmost left concrete node at $x = 0$ is fixed. The tensile failure of the concrete or the yarn segments is restricted to one element per iteration, which prevents simultaneous failure of a series of elements in the case of constant or nearly constant stresses in the longitudinal direction. Furthermore, this guarantees a correct description of the stress transfers between the concrete and the reinforcement in states of ongoing cracking. The Broyden–Fletcher–Goldfarb–Shanno (BFGS) approach [15,16], which is a Quasi-Newton method, in combination with line search is used as iteration method [17], as this shows a good convergence behavior especially with high stress relief in case of filament failure. A discretization of 5000 elements with an element length of $\Delta L = 0.1$ mm and a displacement increment of $\Delta u = 5 \times 10^{-3}$ mm per loading step were used in the following computations. Finer discretizations do not lead to remarkable changes in the results.

4. Numerical calculations on a tension plate

Computations are performed based on the described model to simulate the stress–strain behavior of the tension plates presented in Section 2. Firstly, the case of the so-called ideal yarn is described because it shows major differences between the experimental and the computed behavior of the tension plate. Afterwards, results of models with the microscopic deficiency mechanisms broken bond, waviness, slip and premature filament failure are presented. These results are compared to experimental data to investigate the influence of each mechanism on the macroscopic structural behavior.

4.1. Ideal yarn

An ideal yarn is assumed as homogeneous over its cross-section and continuously connected to the concrete component along the longitudinal direction. Due to the homogeneity the corresponding model has one yarn segment, see Fig. 7, with a cross-sectional area $A^{11} = A = n_y \cdot A_y = 15.4\ \text{mm}^2$ and a circumference $C^{11} = n_y \cdot 6\sqrt{\pi A_y}$ according to Eq. (4) with $\omega = 3$, $\psi = 1$. Furthermore, the weight coefficients reduce to $\alpha^{11} = 1$, see Eq. (1), and $\beta^{11}_{CF,t} = 1$, see Eq. (3) for ideal yarns. Thus, the force of bond elements for one yarn segment is

$$\overline{T}_t^{11} = \Delta L \cdot n_y \cdot 6\sqrt{\pi A_y} \cdot h_{CF}(s_t^{11}), \tag{11}$$

see Eq. (10). The bond law h_{CF} is given by Fig. 6 and the parameters of Table 3. The computation is performed according to the procedure described in Section 3.4.

In Fig. 11, the computed stress–strain relation is shown with the mean stress, which is the total load related to the plate's cross-section and the mean strain of the measurement length of 200 mm according to Fig. 3. Again, the typical behavior can be seen with the uncracked state I, the formation of concrete cracks in state IIa and the increasing load in state IIb where cracking has finished to a large extent. Out of this loading history a typical loading step, e.g. step 1000 with a mean strain of 1.3% and a mean stress of 23 MN/m^2 will be described in detail. Fig. 12 shows the computed concrete stresses along the longitudinal section in the range of $0.2\ \text{m} \leqslant x \leqslant 0.3\ \text{m}$. Cracks are indicated by zero concrete stresses while the concrete has a tensile stress between adjacent cracks but this does not

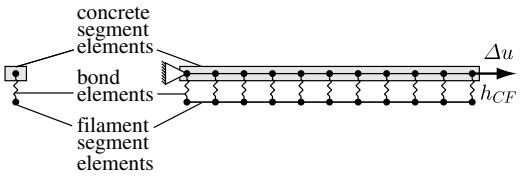

Fig. 7. FE-model for the ideal yarn; schematic.

exceed the tensile strength. The computed crack spacing at ultimate load is ranging from 3.9 mm to 7.8 mm. The first value indicates a bond efficiency of nearly 1 and approaches the smallest possible value, see Eq. (8). The second value, occurring at a few places, still gives room for new cracks.

The reinforcement behavior has a complementary characteristic with peak values at the cracks and minimum values in between, as it can be seen in Fig. 12. Concrete and reinforcement are coupled by bond stresses, which are also shown in Fig. 12. A characteristic behavior is given by a sign reversal of bond stresses across a crack while absolute bond stress values, to a large extent, reach the prescribed limits with a steep transition within a short distance between adjacent cracks. In the case of the ideal yarn, failure of the tension plate occurs if the yarn segment reaches the filament tensile strength, see Table 2. The tension plate fails at a mean strain of 2.7% and a mean stress of 44 MN/m^2, see Fig. 11.

This is beyond the failure point with a strain of 1.3% and a stress of 19 MN/m^2 of the corresponding experimental tension plate, which is also given in Fig. 11. In addition to this large difference in the failure point, there is also a considerable difference in the stiffness in the cracked state IIb. Obviously, the theoretical load carrying capacities of the filaments are by far not exploited in practical applications. Consequently, it has to be concluded that the model of the ideal yarn is obviously not appropriate for a realistic description of textile reinforced concrete. Some possible reasons have been discussed in Section 2, for example the premature failure of filaments or the lower tensile strength of a yarn compared to a filament.

4.2. Non-ideal yarn

In this section, mechanical models for different so-called deficiency effects are discussed. Major mechanisms, which impair the optimal performance, have been described in Section 2. Within the uniaxial framework the corresponding effects are modeled by variations of the general mechanical model given in Section 3.1, see Fig. 5. In order to improve the basic understanding of the structural behavior of textile reinforced concrete these effects – broken bond, waviness, slip and premature filament failure – are modeled as simple as possible and are treated independently from each other in a first approach. In each case, the extent of deficiency is measured by a parameter δ. As the values of this parameter are not precisely known from experimental investigations, a parametric study is performed in each case to investigate the sensitivity of the behavior of the tension plate on each effect.

4.2.1. Yarn with broken bond

A single filament is not continuously connected to the concrete matrix but has parts around its surface, which can be regarded as void in this context. This may be modeled similar to the ideal yarn with a single yarn segment.

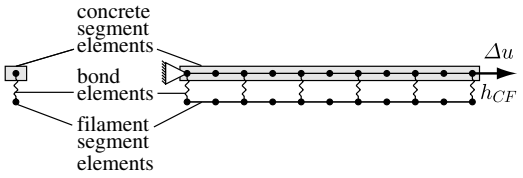

Fig. 8. FE-model for the yarn with broken bond; schematic.

Unlike the case of the ideal yarn not all dedicated nodes of the concrete component and the yarn segment are connected with bond elements, see Fig. 8. The filament–concrete bond law h_{CF} is assumed as bond characteristic, with Eq. (11) being applied to each bond element. The ratio of non-connected node pairs related to all node pairs is used as deficiency parameter δ_1. For reasons of simplicity a regular pattern is assumed, e.g. with $\delta_1 = 1/4$ three connected node-pairs are followed by an unconnected one in a repeated sequence.

Computed stress–strain relations with mean stresses versus mean strains are shown in Fig. 13 with different values of the parameter δ_1 assumed ranging from 1/2 to 3/4. Only slight differences can be seen between the ideal reference case and the deficiency case with $\delta_1 = 1/2$ and $\delta_1 = 2/3$. These cases fail while reaching the tensile strength of the yarn segment. This is different in the case of $\delta_1 = 3/4$ where a bond failure occurs at lower filament stresses when the filament segment slips through suddenly. This is involved with large slip values leading to residual bond stresses, see Fig. 6, and an unloading of the yarn segment while the prescribed displacements of the plate's ends are still increasing. In any of these cases of broken bond, crack spacing at maximum load corresponding to the final cracking state become larger compared to the reference case with values ranging from 10 to 30 mm as the bond efficiency strongly decreases with increasing values of δ_1.

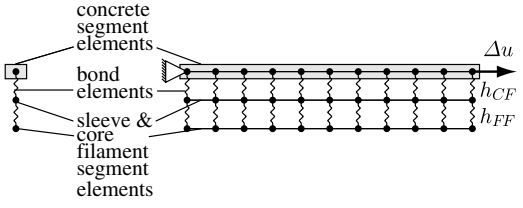

Fig. 9. FE-model for the yarn with slip; schematic.

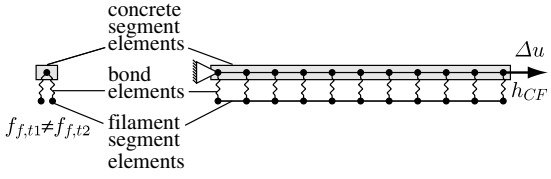

Fig. 10. FE-model for the yarn with premature filament failure; schematic.

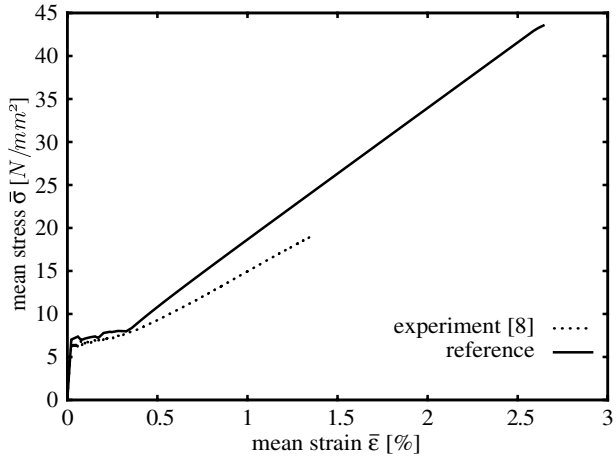

Fig. 11. Computed stress–strain relation of a tension plate with ideal yarn.

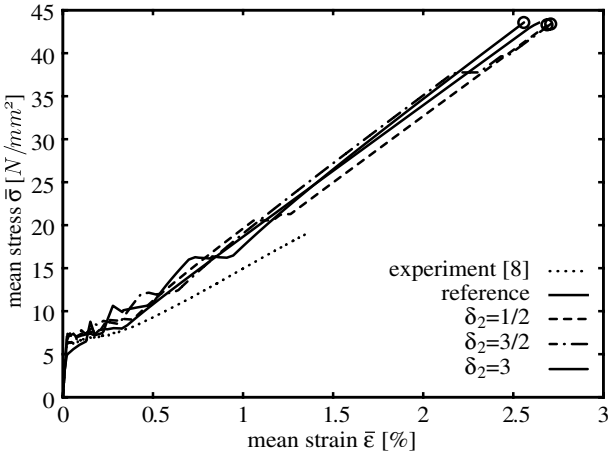

Fig. 14. Computed stress–strain relations with waviness.

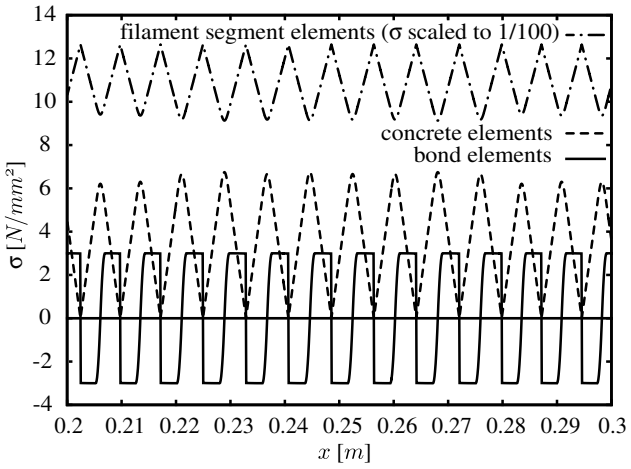

Fig. 12. Computed stresses along longitudinal section 0.2 m $\leqslant x \leqslant$ 0.3 m.

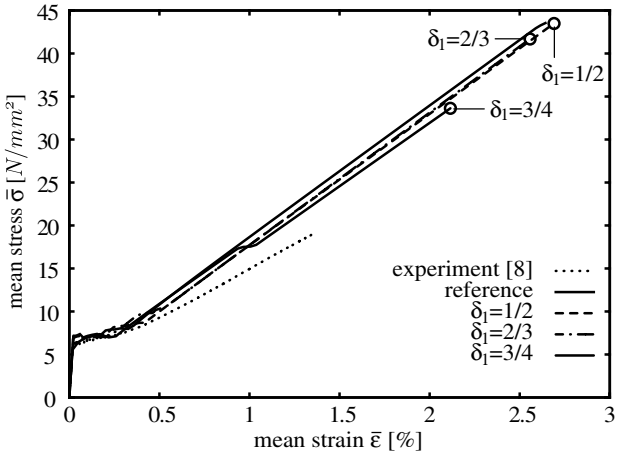

Fig. 13. Computed stress–strain relations with broken bond.

4.2.2. Yarn with waviness

In their initial state, filaments in a yarn are not, in a general sense, perfectly parallel to each other. Looking at a single filament's position, it might have some varying deviation from the straight yarn axis, which is called waviness here. It leads to a stressless deformation prior to the first uniaxial loading in the yarn's axial direction, during which the waviness is straightened. This case is also modeled similar to the ideal yarn (Fig. 7) but the bond law $h_{\mathrm{CF,Ref}}$ is replaced by the bond law $h_{\mathrm{CF,Wav}}$ (Fig. 6), which has a horizontal shift in the direction of the positive slip axis. The deficiency parameter δ_2 is defined for this case as $\delta_2 = s_0/s_{\max}$.

Stress–strain relations are shown in Fig. 14 for the reference case and the cases with values in the range of (1/2)–3 for δ_2. While the reference case has a single major plateau of cracking directly following initial cracking, the cases with waviness are characterized by multiple plateaus of cracking at higher load levels. These load levels increase with increasing values of δ_2. Stiffnesses, ultimate loads and strains remain nearly unchanged compared to the reference state. The computed cracks show a quite regular pattern for the three waviness cases, with crack spacing in the final cracking state at the maximum load ranging from 4.6 to 4.7 mm.

4.2.3. Yarn with slip

Loading has to be transmitted from sleeve filaments to core filaments, where filament–filament bond is activated. In a first approach, this is modeled with two yarn segments. The sleeve segment is directly connected to the concrete component with concrete–filament bond, and the core segment is connected to the sleeve segment with filament–filament bond, see Fig. 9. The deficiency parameter δ_3 is defined as the ratio of the cross-sectional area of the core segment related to the cross-sectional area of the total yarn. In connection with Eq. (1) this leads to cross-sectional areas

$$A^{11} = (1-\delta_3)\cdot A, \quad A^{21} = \delta_3 \cdot A, \tag{12}$$

where the index 11 marks the upper sleeve section and the index 21 marks the lower core section. Regarding the

circumferences, it is assumed that the sleeve segment has the same area in contact with the concrete as the homogeneous ideal yarn. According to Eq. (4) this leads to $C^{11} = n_y \cdot 6\sqrt{\pi A_y}$ with $\omega = 3$ and a shape factor $\psi = 1/\sqrt{1-\delta_3}$ for the annulus. Furthermore, it is assumed that the sleeve segment is completely embedded in the concrete leading to $\beta^{11}_{CF,t} = 1$, $\beta^{11}_{FF,t} = 0$. Finally, the circular core should be completely embedded in the circular sleeve. Thus, we have $C^{21} = n_y \cdot 6\sqrt{\delta_3 \cdot \pi A_y}$ with a shape factor $\psi = 1$ for the circle. The weighting coefficients are chosen with $\beta^{21}_{CF,t} = 0$, $\beta^{21}_{FF,t} = 1$, as the core is assumed to be only in contact with the sleeve. With Eq. (10) applied to the top interfaces the forces of bond elements are given by

$$\overline{T}^{11}_t = \Delta L \cdot n_y \cdot 6\sqrt{\pi A_y} \cdot h_{CF}(s^{11}_t),$$
$$\overline{T}^{21}_t = \Delta L \cdot n_y \cdot 6\sqrt{\pi A_y} \cdot \sqrt{\delta_3} \cdot h_{FF}(s^{21}_t) \quad (13)$$

with the slip s^{11}_t between the concrete and the sleeve segment, the slip s^{21}_t between the sleeve and the core segment and the bond laws h_{CF}, h_{FF} determined by Table 3.

The computations show that the sleeve segment stresses are considerably higher compared to the core segment stresses at the transition to the supported part of the plate where the concrete is not permitted to crack. This transition turns out as area of stress concentration. Failure of the whole plate occurs as the filament tensile strength is reached in this stress concentration area. Stress–strain relations for the case of slip are shown in Fig. 15 for the reference case and different values of the deficiency parameter δ_3 in the range of (1/4)–(3/4). It can be seen that ultimate stresses and strains decrease with an increasing ratio of core segments, because stress concentrations in the sleeve segment become more pronounced. On the other hand, only small differences in the tension plate stiffness can be seen between the slip cases and the reference cases before failure. The computed numbers of cracks decrease with increasing deficiency parameters δ_3. Thus, the respective mean crack spacing increases. However, this effect is only weakly pronounced.

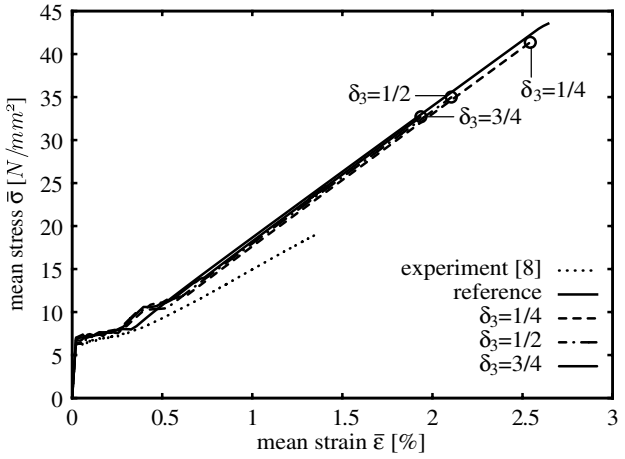

Fig. 15. Computed stress–strain relations with slip.

4.2.4. Yarn with premature filament failure

Glass in general and filaments in particular are sensitive against small defects on their surface, which lead to brittle failure. Such defects may be caused by the mechanical environment, e.g. lateral pressure concentrations, the impaction of solid concrete constituents or the highly reactive chemical environment [6]. Consequently, a number of filaments may not reach their potential tensile strength, as given in Table 2, but will fail at lower tensile stresses. This is again modeled with two yarn segments both having the characteristics of a sleeve segment. Thus, both segments are directly connected with the concrete component with concrete–filament bond while the second yarn segment has a lower tensile strength, see Fig. 10. The deficiency parameter δ_4 is defined as ratio of the cross-sectional area of the early failing segment to the cross-sectional area of the total yarn. This results in a similar cross-sectional area as in the case of the yarn with slip, see Eq. (12), but with segments arranged in one row with two columns

$$A^{11} = (1-\delta_4) \cdot A, \quad A^{12} = \delta_4 \cdot A \quad (14)$$

and the early failing segment in the second column. The circumference of the whole yarn is given by $C = 2\psi\omega\sqrt{\pi A}$ according to Eq. (4) with a roughness coefficient $\omega = 3$ and a shape coefficient $\psi = 1$. As both segments are considered as sleeve segments, their circumference is also scaled according to Eq. (14) with $C^{11} = n_y \cdot (1-\delta_4) \cdot C = n_y \cdot 6(1-\delta_4)\sqrt{\pi A_y}$ and $C^{12} = n_y \cdot \delta_4 \cdot C = n_y \cdot 6\delta_4\sqrt{\pi A_y}$. For reasons of simplicity, it is assumed that the two segments do not interact with each other and that each segment is fully embedded in the concrete. This leads to weighting coefficients $\beta^{11}_{CF,t} = \beta^{12}_{CF,t} = 1$ and $\beta^{11}_{FF,t} = \beta^{12}_{FF,t} = 0$ respectively. Finally, this results in bond forces

$$\overline{T}^{11}_t = \Delta L \cdot n_y \cdot 6(1-\delta_4)\sqrt{\pi A_y} \cdot h_{CF}(s^{11}_t),$$
$$\overline{T}^{12}_t = \Delta L \cdot n_y \cdot 6\delta_4\sqrt{\pi A_y} \cdot h_{CF}(s^{12}_t)$$

according to Eq. (10) applied to the top interfaces, with the slip s^{11}_t between the concrete and the normal failing segment and the slip s^{12}_t between the concrete and the early failing segment. Beside the deficiency parameter δ_4, a further parameter, the reduced strength of the early failing filaments, has to be considered. A random distribution of the tensile strength has to be expected but reliable experimental data about types and parameters of strength distributions of filaments embedded in the concrete are currently not available. In a first approach, a reduced tensile strength with the value $f_{f,t} = 300\ \mathrm{MN/m^2}$ for the early failing segment is chosen for the computations based on the assumption that a certain amount of reinforcement fails simultaneously with the concrete.

Corresponding stress–strain relations are shown in Fig. 16 for different values of the deficiency parameter δ_4 ranging from 1/6 to 1/2. Obviously, both the stiffness and the ultimate load of the tension plate are inversely proportional to the ratio of the early failing segments while the ultimate strains show only minor changes. The crack spacing in

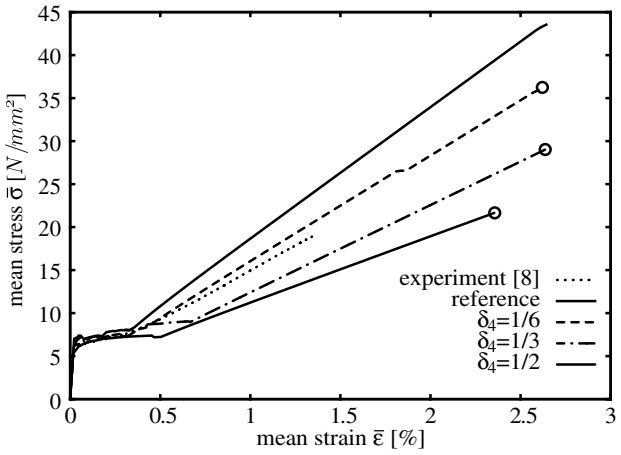

Fig. 16. Computed stress–strain relations with premature filament failure.

the final cracking state at maximum load for the case of a small deficiency parameter $\delta_4 = 1/6$ show values in the range of 4.7–7.8 mm, similar to those of the ideal yarn. With increasing values of δ_4, the crack spacing increase as well. For example, for $\delta_4 = 1/2$, the crack spacing show values ranging from 13.9 to 15.3 mm. The strong influence of early failing segments supports the assumption that there is also an influence of the reduced filament tensile strength $f_{f,t}$. Computations with varying values of $f_{f,t}$ show that this applies to the intermediate phase of cracking while the stiffness in the final cracking state as well as the ultimate stress and strain of the tension plate nearly remain unchanged.

5. Conclusions

Concerning the ultimate state, the structural behavior of tension plates with uniaxial textile reinforcement may on a macroscopic level be characterized by the

– limit load,
– strain at limit load,
– stiffness in the final cracking state,
– crack spacing in the final cracking state.

An ideal case with homogeneous, uniform reinforcement is used as reference with an optimal structural performance. However, experimental investigations for actual plates show a considerable decrease with respect to limit load, limit strain and stiffness. Thus, a range of deficiency mechanisms has been numerically investigated to see their effects on the structural behavior. As a major result, it can be seen that stiffness degradation is mainly caused by premature filament failure. This particular deficiency mechanism also leads to decreasing limit loads but the limit strains almost remain unchanged compared to the reference case. A decreasing limit load is also caused by the slippage mechanism of core filaments. This is connected with decreasing limit strains, but the stiffness in the cracked state nearly remains unchanged compared to the reference case. A reduction of the limit load and limit strain may also be caused by partially broken bond between filament and concrete but there is only a minor influence on the stiffness in the cracked state. Furthermore, a strong increase in the crack spacing is calculated for broken bond compared to all other cases. Finally, waviness with a stressless deformation prior to initial loading shows a different cracking behavior on the way to the final cracking state. However, there are no essential differences with respect to limit loads, limit strains and stiffnesses compared to the reference case.

In principle, all these mechanisms should influence the structural behavior of the tension plate to a more or less extent but the results show that mainly a combination of premature filament failure and slippage of core filaments should cause the observed decrease of the limit load, the limit strain and the stiffness compared to an optimal behavior. A combination of both should be used for further extensions of the matrix scheme of the uniaxial model.

An essential problem is currently the estimation of the values of the deficiency parameters, which have to be regarded as micromechanical. Because of the microscopic scale, the determination of these values is difficult. This may be the reason why corresponding experimental data is currently rare and, if available, such values show high scatter. Nevertheless, for modeling they have to be estimated or identified by means of reverse engineering. In this sense, the presented model in principle offers the possibility to model a broad range of experiments, such as the tensile tests or pullout tests for both filaments or whole yarns considered in this study. Furthermore, it is also possible and necessary to include stochastic effects in the model. Concerning the modeling of textile structures, different from the unidirectional reinforcement treated in this contribution, it is probably necessary to take into account the transverse reinforcement.

Acknowledgements

The authors gratefully acknowledge the financial support of this research from Deutsche Forschungsgemeinschaft DFG (German Research Foundation) within the Sonderforschungsbereich 528 (Collaborative Research Center) "Textile Reinforcement for Structural Strengthening and Retrofitting" at Technische Universität Dresden as well as their colleagues for providing all experimental data.

References

[1] Curbach M, Jesse F. Verstärken von Stahlbetonbauteilen mit textilbewehrtem Beton–Kurzer Bericht zu aktuellen Entwicklungen. Beton- und Stahlbetonbau 2005;100(S1):78–81.
[2] Brückner A, Ortlepp R, Weiland S, Curbach M. Textile structures for shear strengthening. In: Alexander MA, Beushausen HD, Dehn F, Moyo P, editors. Proceedings of the international conference on concrete repair, rehabilitation and retrofitting (ICCRRR) – CD-ROM. Cape Town, South Africa: Taylor & Francis/Balkema; 2006. p. 1225–30.
[3] Hempel R, Schorn H, Franzke G, Helbig U. Textile reinforced concrete with AR-glass–fibre-multifilament yarn – a new innovative compound material for concrete repair and rehabilitation. In:

Alexander MA, Beushausen HD, Dehn F, Moyo P, editors. Proceedings of the international conference on concrete repair, rehabilitation and retrofitting (ICCRRR) – CD-ROM. Cape Town, South Africa: Taylor & Francis/Balkema; 1999. p. 1081–6.

[4] Hempel R, Butler M, Proske D, Franzke G, Engler T. Strengthening of concrete masts using multi-axial AR-glass structures. In: Alexander MA, Beushausen HD, Dehn F, Moyo P, editors. Proceedings of the international conference on concrete repair, rehabilitation and retrofitting (ICCRRR) – CD-ROM. Cape Town, South Africa: Taylor & Francis/Balkema; 2006. p. 1131–7.

[5] Hegger J, Will N, Schneider HW, Kölzer P. New components of textile reinforced concrete. Beton- und Stahlbetonbau 2004;99(6): 482–7 [in German].

[6] Schorn H, Schiekel M. Prediction of lifetime of alkali-resistant glass fibres in cementitious concretes. In: di Prisco M, Felicetti R, Plizzari GA, editors. 6th RILEM symposium on fibre-reinforced concretes (FRC) – BEFIB 2004, vol. 1. Varenna, Italy: RILEM; 2004. p. 615–24.

[7] Jesse F, Curbach M. Strength of continuous AR-glass fibre reinforcement of cementitious composites. In: Naaman AE, Reinhardt HW, editors. High performance fiber reinforced cement composites (HPFRCC4). Ann Arbor, USA: RILEM; 2003. p. 337–48. June.

[8] Jesse F. Load bearing behaviour of filament yarns in a cementitious matrix. PhD thesis. Technische Universität Dresden, Dresden, 2004 [in German].

[9] Molter M. Zum Tragverhalten von textilbewehrtem Beton. PhD thesis. Aachen, RWTH Aachen, 2005.

[10] Ohno S, Hannant DJ. Modeling the stress–strain response of continuous fiber reinforced cement composites. ACI Mater J 1994;91(3):306–12.

[11] CEB-FIP Model Code 1990. Thomas Telford Services Ltd., London, 1998.

[12] Zastrau B, Richter M, Lepenies I. On the analytical solution of pullout phenomena in textile reinforced concrete. J Eng Mater Technol 2003;125:38–43.

[13] Banholzer B, Brameshuber W, Jung W. Analytical simulation of pull-out tests – the direct problem. Cement Concr Compos 2005;27: 93–101.

[14] Zhandarov S, Mäder E. Characterization of fiber/matrix interface strength: applicability of different tests, approaches and parameters. Compos Sci Technol 2005;65:149–60.

[15] Matthies H, Strang G. The solution of non-linear finite element equations. Int J Numer Methods Eng 1979;14:1613–26.

[16] Nocedal J, Wright SJ. Numerical optimization. New York: Springer-Verlag; 1999.

[17] Bathe KJ. Finite element procedures. Englewood Cliffs, New Jersey: Prentice-Hall; 1996.